PHYSICAL REVIEW B VOLUME 53, NUMBER 2 1 JANUARY 1996-II

Exchange interactions and magnetism of Co^{2+} in $Zn_{1-x}Co_xTe$

M. Zielinski, C. Rigaux, A. Lemaître, and A. Mycielski*
Groupe de Physique de Solides, Universités Paris VII et Paris VI, 2, place Jussieu, 75251 Paris Cedex 05, France

J. Deportes
Laboratoire Louis Néel, Grenoble, France

(Received 29 June 1995)

A study of cobalt-carrier exchange interactions is carried out in very dilute $Zn_{1-x}Co_xTe$ ($x \leqslant 1\%$) from correlated magneto-optical and magnetization measurements at $T=1.8$ K. The resonant magneto-optic Kerr effect is used to complement magnetoreflectance experiments, and determine precisely the exciton Zeeman splittings on single crystals of various Co compositions. Correlated measurements of magnetization performed *on the same samples* provide a determination of exchange integrals for Γ_6 and Γ_8 bands within the framework of the exchange model based on the mean-field approximation. In the investigated field and composition range, we find $N_0\alpha=0.31\pm0.03$ eV; $N_0\beta=-3.03\pm0.15$ eV. This abnormally large value of the p-d exchange constant does not vary with Co concentration in the investigated region. Low-temperature magnetization data obtained in fields up to 15 T are consistently interpreted in a model including the contributions of isolated ions and Co^{2+}-Co^{2+} pairs of second and third neighbors for the values of exchange constants previously determined. Antiferromagnetic interactions between more distant ions than third neighbors are also taken into account. The long-range exchange parameters obtained by using either a modified Brillouin function or a mean-field approach are in good agreement.

I. INTRODUCTION

Great interest has been recently devoted to semimagnetic semiconductors where Co^{2+} ions are diluted in II-VI compounds.[1] Different experimental techniques have been used to study the magnetic exchange interactions between Co^{2+} ions in compounds of zinc-blende and wurtzite[2–7] structure. This class of materials differs from other semimagnetic semiconductors by the strength of their magnetic interactions. Typically, the antiferromagnetic nearest-neighbor (NN) exchange parameter J_1 is about four times larger than in Mn-based DMS.[1] In contrast, only a few results have been so far reported about the cobalt-carrier exchange interactions in II-VI compounds. Studies were carried out in $Cd_{1-x}Co_xSe$, of wurtzite structure. Conduction and valence exchange integrals ($N_0\alpha=0.279$ eV, $N_0\beta=-1.873$ eV) were determined from magnetoreflectance and magnetization experiments.[8] A slightly larger value of $N_0(\alpha-\beta)$ (2.52 eV) was obtained from high-field measurements on a more diluted compound.[9] Recent studies of spin-flip Raman scattering and magnetization confirm the composition dependence of the p-d antiferromagnetic exchange integral.[10] A systematic increase of $|N_0\beta|$ is observed on decreasing the Co composition.

For Co-based DMS of zinc-blende structure, only the difference between exchange constants was determined from correlated magnetoreflectance and magnetization measurements [$N_0(\alpha-\beta)=1.62$ eV for CdCoTe (Ref. 11) and 2.42 eV for ZnCoSe (Ref. 12)]. These scarce data however underline the strong ion-carrier exchange interactions in Co-based compounds in comparison with the data previously reported for Mn and Fe DMS of identical host lattice.

In this paper we focus our interest on the compounds $Zn_{1-x}Co_xTe$, of zinc-blende structure. We present a systematic study of the magnetization, magnetoreflectance, and magneto-optic Kerr effect (MOKE) carried out at $T=1.8$ K on very dilute compounds ($x \leqslant 1\%$). The large Kerr rotation observed in the region of the exciton transition offers a useful method for a precise determination of the Zeeman spectrum, especially at low field. The high dilution regime is of particular interest[13] to check the validity of the exchange model based on the mean-field approximation[14] for the determination of the Co-carrier exchange parameters.

The magnetic properties of diluted $Zn_{1-x}Co_xTe$ compounds were previously investigated. The NN exchange constant, $J_1/k_B=-38$ K, was established from neutron-scattering experiments.[6] Magnetization steps observed at very low temperature have provided the exchange constants $J_2/k_B=-5.7$ K and $J_3/k_B=-2.7$ K between second and third neighbors, respectively.[7] On the basis of these results we present an analysis of magnetization data obtained up to 15 T in the temperature range 1.5–15 K.

II. EXPERIMENTS

$Zn_{1-x}Co_xTe$ single crystals were grown by a modified Bridgman method. The Co molar fraction was determined by x-ray fluorescence with a relative uncertainty of 10%. For each sample the energy of the exciton state E_0 was determined from the position of the reflectivity structure at $T=1.8$ K. $E_0(x)$ is well described by the linear relation

$$E_0(x)=(2.3802\pm0.0005)+(1.52\pm0.07)x \quad \text{(eV)} \tag{1}$$

deduced from a least-squares fit of the data in the composition range $x \leqslant 1\%$ (Fig. 1). The exciton energy in

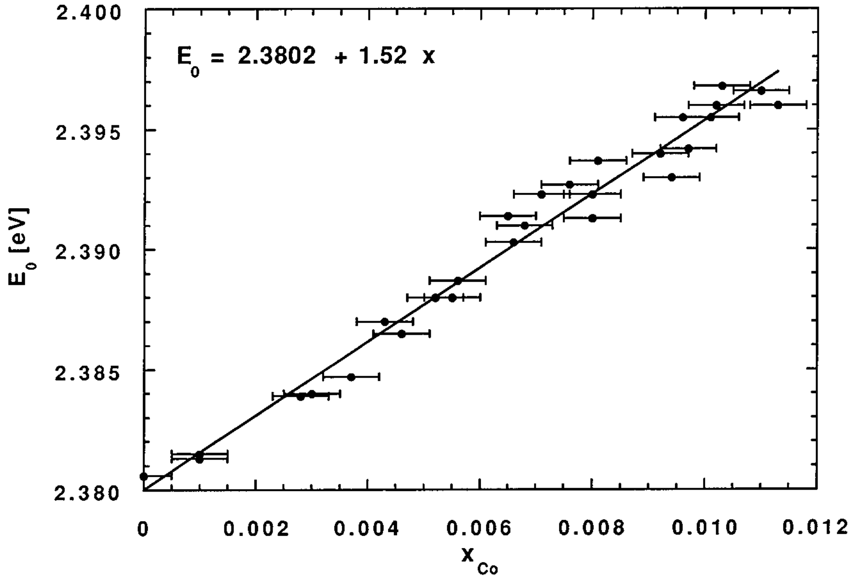

FIG. 1. Composition dependence of the exciton energy at $T=1.8$ K. x is determined by x-ray fluorescence. The straight line corresponds to the least-squares linear fit [Eq. (1)].

$Zn_{1-x}Co_xTe$ increases twice as fast with the concentration of the magnetic ions, than in $Zn_{1-x}Mn_xTe$ compounds at the same temperature.[15]

The exciton Zeeman spectrum of $Zn_{1-x}Co_xTe$ compounds was studied at temperature $T=1.8$ K by magnetoreflectance experiments performed in the Faraday configuration with circularly polarized light ($\sigma^{\pm}$) in fields up to 6.5 T. Kerr rotation spectra were also used to determine precisely the energies of magneto-optical transitions. A sensitive modulation technique is used for measurements of the magneto-optical Kerr effect (MOKE). The experimental method is very similar to that described in Ref. 16. Optical experiments were made on cleaved (110) planes or on polished and etched samples. Magnetization measurements were carried out *on the same samples*, at $T=1.8$ K in fields up to 5 T, by the use of a superconducting quantum interference device (SQUID) magnetometer. Additional high-field measurements (up to 10 or 15 T) have been performed by an extraction method, at temperatures between 1.5 and 15 K.

III. MAGNETIZATION

The energy spectrum of $3d^7$ electrons of a Co^{2+} ion in a cubic crystal has been studied by Villeret, Rodriguez, and Kartheuser.[17] In a tetrahedral crystal field the free-ion ground state $^4F_{9/2}$ is split into an orbital singlet $^4A_2$ and two higher-lying orbital triplets $^4T_2$ and $^4T_1$. The first excited state is separated from $^4A_2$ by $\Delta \approx 3450$ cm^{-1} for ZnCoTe.[18] The magnetism of Co^{2+} in ZnTe is then governed by the $^4A_2$ ground state, a quartet of spin $S=3/2$ and zero orbital momentum. The gyromagnetic factor $g=2.2972$ was determined from electron-spin resonance.[19] The paramagnetism of isolated Co^{2+} ions is described by a Brillouin function for a spin $S=3/2$. This situation is similar to that of Mn^{2+} ions with $S=5/2$.

The magnetization of Co^{2+} in $Zn_{1-x}Co_xTe$ alloys of different compositions is illustrated in Figs. 2–4. The diamagnetic contribution of the lattice, $\chi_d=-3.05\times10^{-7}$ emu/g (3.8310^{-6} SI), obtained from our measurements on ZnTe has

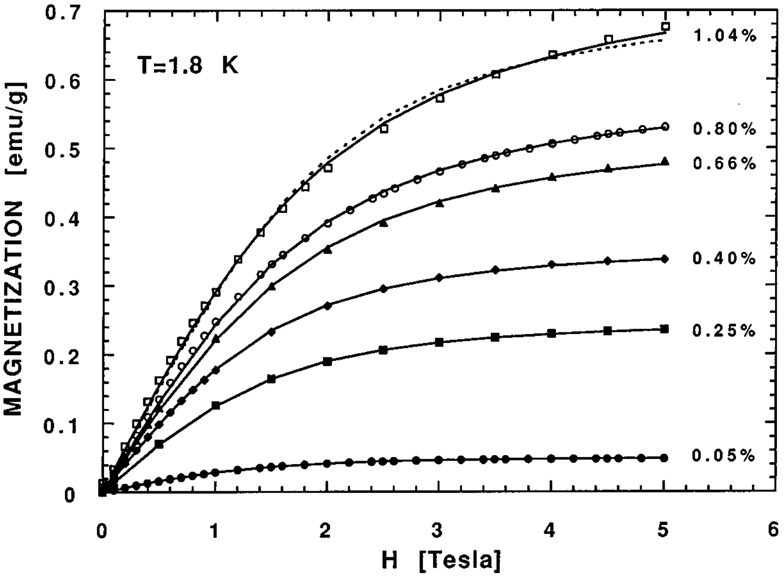

FIG. 2. Magnetization curves at $T=1.8$ K for samples of different compositions (x_{opt} is indicated on each curve). Symbols are the experimental data. Solid line is the theoretical fit according to Eq. (2), using modified Brillouin function (Fit A). Dashed line is the theoretical fit according to Eq. (2), using MFA (Fit B). Parameters obtained from the fits are reported in Table I (Fit A:x_m,T_0; Fit B:x_m,I).

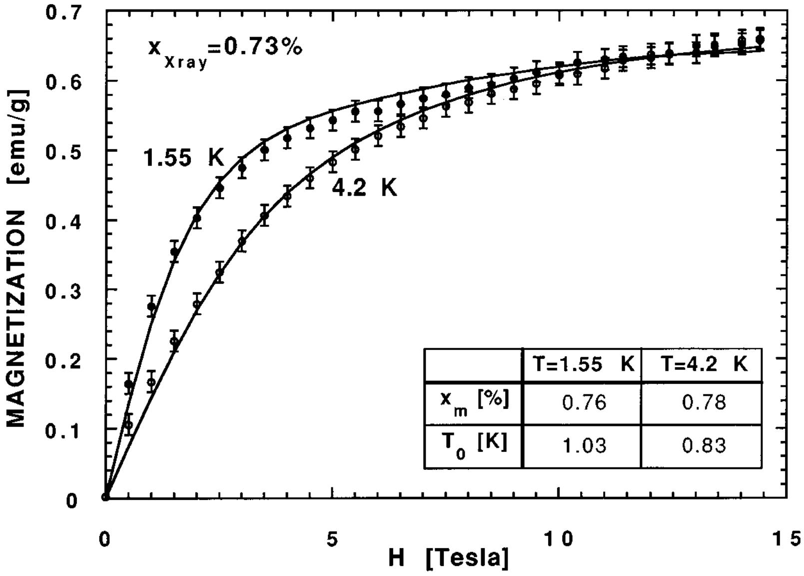

FIG. 3. Magnetization curves at $T=1.55$ and 4.2 K. $x_{\text{x-ray}}=0.73\%$. Symbols are the experimental data. Solid lines are the theoretical fits, according to Eq. (2) (Fit *A*). Best-fit parameters are reported on the plot.

been subtracted from the data. Magnetization curves $M(H)$ obtained from SQUID measurements on alloys of several compositions, at $T=1.8$ K, are reported in Fig. 2. The Co molar fraction (from 0.05 to 1%) is deduced from the position of the exciton structure at $T=1.8$ K, using the relation (1). Figure 3 shows magnetization data up to 15 T at $T=1.55$ and 4.2 K, for $x=0.73\%$. The magnetization curves obtained at different temperatures are reported in Fig. 4 for $x=1.06\%$.

At $T=1.8$ K, the magnetization saturates only at low dilutions, typically for $x\leqslant 0.4\%$ (Fig. 2). For higher Co concentrations, the magnetization increases continuously with the magnetic field even in the high-field region (Fig. 3). This behavior drastically contrasts with the data obtained in diluted $\mathrm{Zn}_{1-x}\mathrm{Mn}_x\mathrm{Te}$ (Ref. 15) where, at the same temperature, the saturation is reached in a field of 6 T. The present data cannot be explained solely by the magnetization of isolated Co^{2+} ions. The contribution of small clusters should be also taken into account for a quantitative interpretation of magnetic behavior.

Our model consists in describing the magnetization of diluted alloys as the sum of the contributions of singles and pairs of second and third neighbors. The magnetization per unit mass is

$$M=-\frac{g\mu_B N_A}{m(x)}\,x\langle\langle S_z\rangle\rangle, \tag{2}$$

where $m(x)=(1-x)m_{\mathrm{ZnTe}}+xm_{\mathrm{CoTe}}$ is the molar mass of the compound $\mathrm{Zn}_{1-x}\mathrm{Co}_x\mathrm{Te}$ and N_A is the Avogadro number. $\langle\langle S_z\rangle\rangle$ denotes the thermal as well as spatial average of the spin component S_z along the magnetic field $H\|z$. $\langle\langle S_z\rangle\rangle$ is obtained by weighting the thermal average of the spin compound $\langle S_z\rangle_i$ of each entity by the probability $P_i(x)$ that a Co^{2+} ion belongs to the cluster i:

$$\langle\langle S_z\rangle\rangle=P_1\langle S_z\rangle_1+P_2\langle S_z\rangle_2+P_3\langle S_z\rangle_3 \tag{3}$$

(the index $i=1,2,3$ refers to singles, second-, and third-neighbor pairs, respectively). NN pairs are frozen in the non-

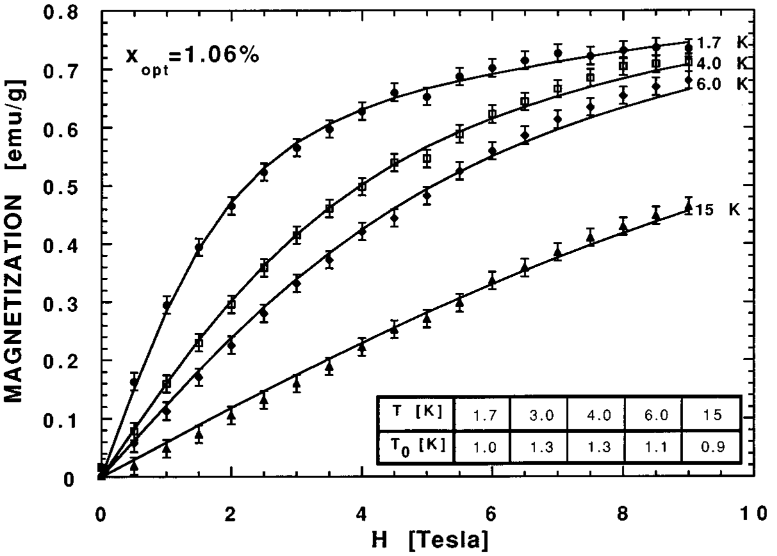

FIG. 4. Magnetization curves at different temperatures. $x_{\text{opt}}=1.06\%$. Symbols are the experimental data. Solid lines are the theoretical fits, according to Eq. (2) (Fit *A*) with $x_m=1.01\%$ and T_0 reported on the plot.

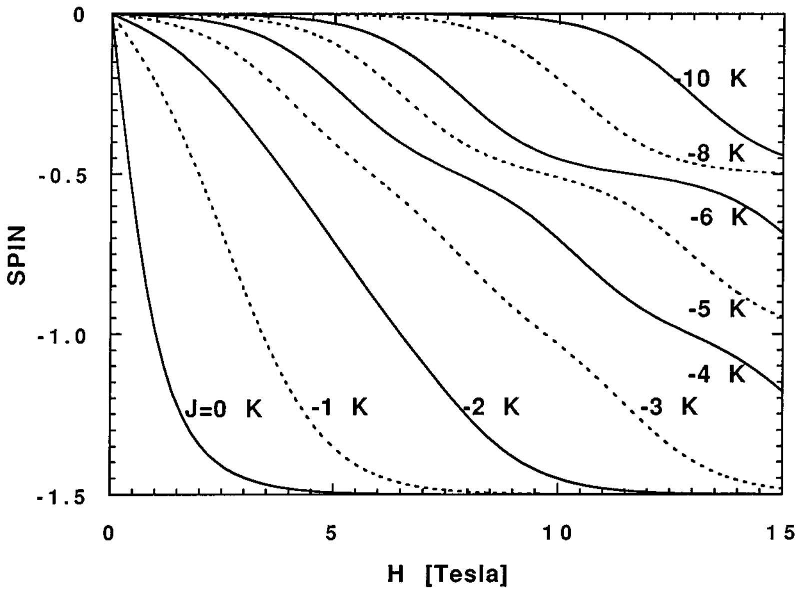

FIG. 5. Mean spin value $\langle S_z \rangle$ vs magnetic field for a Co^{2+} ion in a pair, calculated from Eq. (11) for different values of coupling constant J ($T=1.55$ K).

magnetic ground state and do not contribute to $\langle\langle S_z \rangle\rangle$, since $J_1/k_B \approx -38$ K.[6] For a random distribution of the ions over the fcc lattice, the probability that a Co^{2+} ion is isolated (without first, second and third neighbors) is $P_1=(1-x)^{42}$. The probability that a Co^{2+} ion belongs to a pair is $P_2=6x(1-x)^{62}$ (for NNN pairs) and $P_3=24x(1-x)^{68}$ (for a pair of third neighbors). For the composition $x=0.8\%$, 91% of ions are distributed in these types of clusters (including NN pairs). The contribution of larger clusters (e.g., triplets) is neglected.

The thermal average $\langle S_z \rangle_1$ of an isolated ion is usually described by a modified Brillouin function for a spin $S=3/2$

$$\langle S_z \rangle_1 = -SB_s\left(\frac{Sg\mu_B H}{k_B(T+T_0)}\right), \tag{4}$$

$$B_s(x)=\frac{2S+1}{2S}\coth\left(\frac{2S+1}{2S}x\right)-\frac{1}{2S}\coth\left(\frac{x}{2S}\right). \tag{5}$$

The parameter T_0 accounts phenomenologically for the long-range antiferromagnetic interactions between spins more distant than third neighbors.

An alternative method [previously used in Fe-based DMS (Ref. 20)] consists of treating the antiferromagnetic (AF) interactions between isolated ions in the mean-field approximation

$$\langle S_z \rangle_1 = -SB_s\left(\frac{Sg\mu_B(H-h_m)}{k_B T}\right), \tag{6}$$

where the molecular field h_m is related to $\langle S_z \rangle_1$ by

$$g\mu_B h_m = 2\langle S_z \rangle_1 \sum_{j\geq 4} J_{1j} = \langle S_z \rangle_1 I \tag{7}$$

J_{ij} is the exchange constant between isolated Co ions at sites i and j. For a random distribution, the summation in (7) over

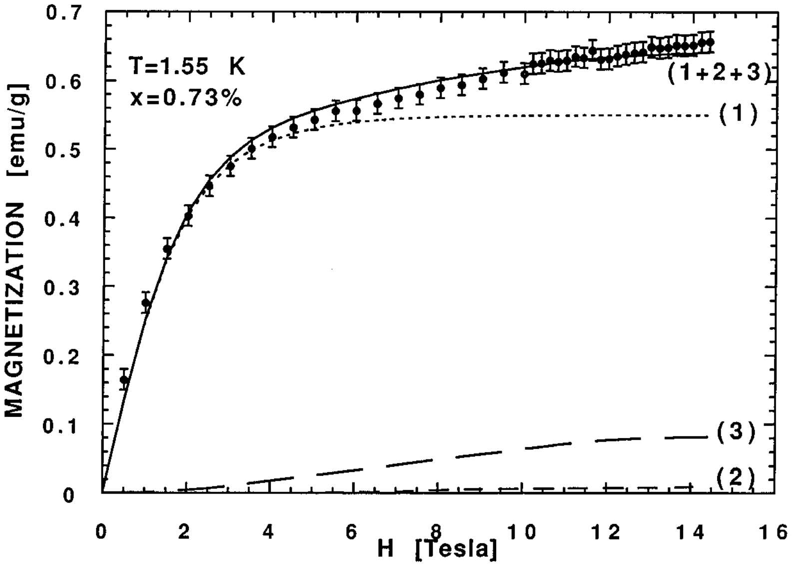

FIG. 6. The different contributions to $M(H)$ calculated from Eqs. (4) and (11). (1) Singles (Fit A, $x_m=0.76\%$, $T_0=1.03$ K); (2) Pairs of second neighbors ($J_2=-5.7$ K); (3) Pairs of third neighbors ($J_3=-2.7$ K); 1+2+3 is the complete theoretical curve compared to experimental data.

TABLE I. Parameters for $Zn_{1-x}Co_xTe$ obtained from magnetization measurements at $T=1.8$ K, $H\leqslant 5$ T. $x_{\rm opt}$ is determined from exciton energy [Eq. (1)]. Fit *A* uses Eqs. (2) and (3) with modified Brillouin function for singles. Fit *B* uses Eqs. (2) and (3) with MFA for singles.

Concentration (%)		Fit *A*		Fit *B*	
$x_{\text{x-ray}}$	$x_{\rm opt}$	x_m (%)	T_0 (K)	x_m (%)	I/k_B (K)
	0.10	0.05	0.03	0.05	−0.02
0.28	0.24	0.26	0.31	0.26	−0.27
		0.40	0.32	0.39	−0.27
0.66	0.66	0.61	0.71	0.59	−0.58
0.71	0.80	0.71	0.72	0.68	−0.60
0.92	1.06	0.94	0.94	0.89	−0.78
1.02	1.04	1.00	0.88	0.94	−0.70

sites occupied by Co ions is replaced by its spatial average over all lattice sites. The parameter I is approximated by

$$I\approx 2xP_1(x)\sum_{\text{all } j\geqslant 4} J_{1j}\,. \tag{8}$$

It has to be determined in order to satisfy the self-consistent equation

$$\langle S_z\rangle_1=-SB_s\left(\frac{S(g\mu_BH-I\langle S_z\rangle_1)}{k_BT}\right). \tag{9}$$

The contributions of the second- and third-neighbor pairs are calculated for the values of the exchange constants given in Ref. 7. The energy levels of a Co pair are

$$E(S_T,m)=-J\left[S_T(S_T+1)-\frac{15}{2}\right]+g\mu_BmH. \tag{10}$$

S_T is a total spin of the pair ($0\leqslant S_T\leqslant 3$) and m is the component of the total spin along H ($-S_T\leqslant m\leqslant S_T$). J is the exchange constant between pair ions. The thermal average of the spin component $\langle S_z\rangle$ per ion is calculated from

$$\langle S_z\rangle=\frac{1}{2}\,\frac{\Sigma_{0\leqslant S_T\leqslant 3}\Sigma_{-S_T\leqslant m\leqslant S_T}m\ \exp(-E(S_T,m)/k_BT)}{\Sigma_{0\leqslant S_T\leqslant 3}\Sigma_{-S_T\leqslant m\leqslant S_T}\ \exp(-E(S_T,m)/k_BT)}\,. \tag{11}$$

Figure 5 shows the $\langle S_z\rangle$ values versus H, at $T=1.55$ K, for different values of coupling constant J. According to these results and taking into account cluster probabilities, one may expect a significant contribution to $\langle\langle S_z\rangle\rangle$ originating principally from third-neighbor pairs (about 10% of the singles contribution at $H=10$ T).

The total magnetization was calculated from expressions (2), (3), (4), and (11) assuming a random distribution of Co^{2+} ions and taking $J_2=-5.7$ K and $J_3=-2.7$ K. The composition x_m and temperature T_0 entering in the theoretical dependence $M(H)$ are determined to obtain the best fits with experimental magnetization data. We have also used the mean-field approach taking composition x_m and I as fitting parameters. The comparison between calculated and experimental magnetization curves is presented in Fig. 2 where the best fits performed within both approaches are reported. The parameters obtained from the fitting procedure are reported in Table I. The quality of the fit is improved when using the modified Brillouin function.

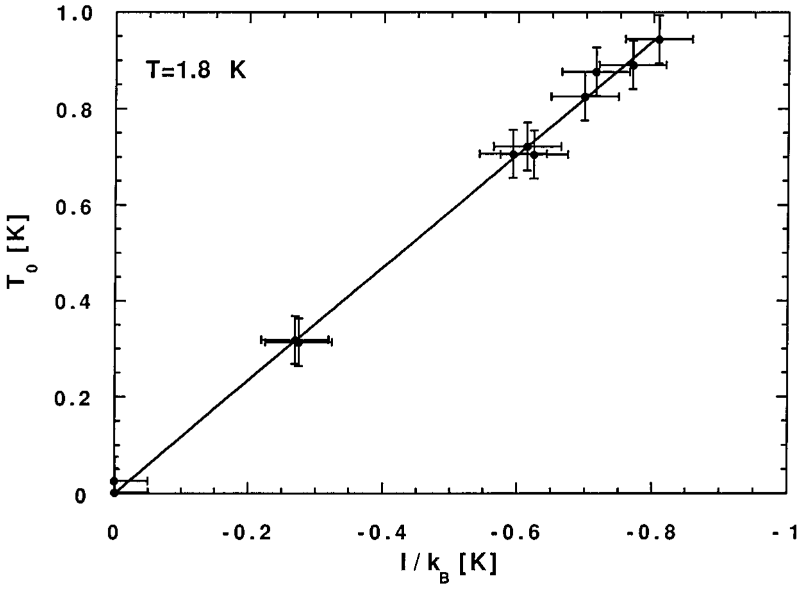

FIG. 7. Parameters $T_0(x)$ vs $I(x)$ deduced from the fits reported in Fig. 2 ($T=1.8$ K).

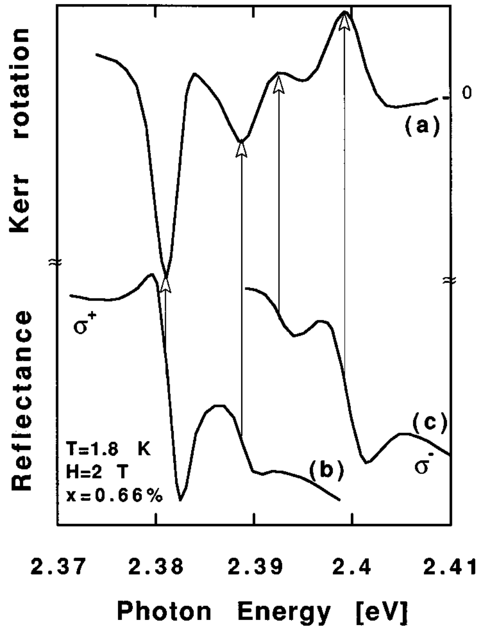

FIG. 8. Kerr rotation spectrum [curve (a)] compared to magnetoreflectance spectra in $\sigma^{\pm}$ polarizations [curves (b) and (c)] ($T=1.8$ K, $H=2$ T, $x_{\rm opt}=0.66\%$). The θ_k peaks correspond approximately to the center of the reflectance structure.

The contribution of singles and pairs included in the present model accounts quantitatively for the cobalt magnetization data, obtained at $T=1.55$ and 4.2 K in fields up to 15 T, within the limit of the experimental accuracy. The comparison between theoretical fits and experimental data is reported in Fig. 3 with the corresponding parameters.

Figure 6 shows the different contributions to $M(H)$ due to singles, second- and third-neighbor pairs, and the comparison of the overall magnetization with the experimental curve obtained for $x=0.73\%$ at $T=1.55$ K. The field dependence in the high-field range results essentially from the magnetization of the third-neighbor pairs. The second-neighbor pairs introduce only a small correction, as it is shown in Fig. 6. The same model also describes satisfactorily the dependence on temperature of magnetization curves presented in Fig. 4.

The cobalt molar fraction x_m obtained from the analysis of the magnetization is quite consistent with $x_{\rm opt}$ deduced from the exciton energy. Two different approaches (modified Brillouin function or mean-field approximation) taking into account long-range AF interactions between isolated ions lead to a determination of the concentration dependence of the I and T_0 parameters. The values obtained from the best fits are reported in Fig. 7. We found $k_BT_0/I=-1.18\pm0.07$ in the high dilution region. This result is consistent with the relation

$$k_BT_0=-\frac{S(S+1)}{3}I \tag{12}$$

deduced from Eq. (8) and the expression of T_0 obtained in the low-field limit[21]

$$k_BT_0=-\frac{2}{3}xP_1(x)S(S+1)\sum_{j\geqslant 4}J_{1,j}. \tag{13}$$

IV. THE MAGNETO-OPTIC KERR EFFECT

Like Faraday rotation, the MOKE results from the magnetic circular birefringence of the crystal. Linearly polarized incident radiation (**E**‖x) propagating in the magnetic-field direction (**H**‖z) becomes elliptically polarized in the (x,y) plane after reflection at the crystal. The Kerr rotation θ_k is the angle of the major axis with the incident polarization direction. The reflection coefficients $r^{\pm}$ associated with the circular eigenmodes $\sigma^{\pm}$ propagating in the crystal are related to θ_k and ϵ_k (Kerr ellipticity) by

$$\frac{r^-}{r^+}=\tan(\pi/4-\epsilon_k)\exp(2i\theta_k). \tag{14}$$

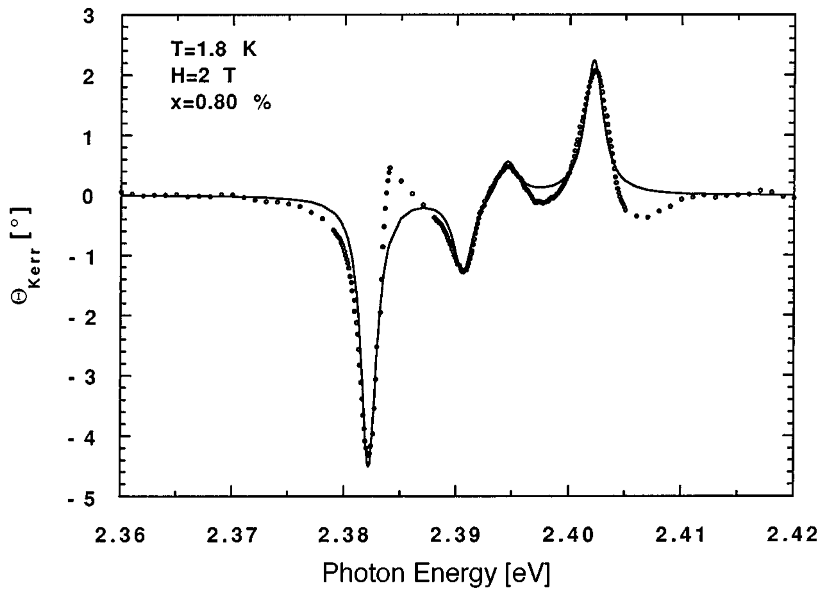

FIG. 9. The comparison of the Kerr rotation calculated from Eq. (20) with the experimental spectrum. Fit is made using damping terms and oscillator strengths as parameters. Symbols are the experimental data. Solid line is the calculated spectrum.

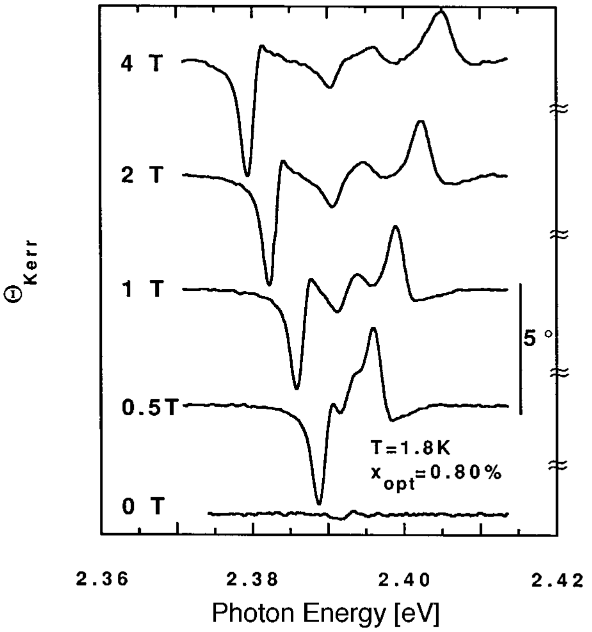

FIG. 10. Kerr rotation spectra for $x=0.80\%$ in different fields at $T=1.8$ K.

The MOKE in DMS is determined from (14) by expressing the Fresnel reflection coefficients in terms of the frequency-dependent dielectric function:

$$r^{\pm}=\frac{1-n^{\pm}}{1+n^{\pm}}. \tag{15}$$

The complex refractive indices $n^{\pm}$ associated with $\sigma^{\pm}$ modes satisfy the relation

$$n_{\pm}^2=\varepsilon_{\pm}=\varepsilon_{xx}\mp i\varepsilon_{xy}, \tag{16}$$

where ε_{xx} and ε_{xy} denote the diagonal and off-diagonal elements of the dielectric tensor of the cubic crystal in the magnetic field.[22]

Using the explicit form of the dielectric tensor elements derived from time-dependent perturbation theory[22] and restricting our interest to photon energies $\hbar\omega$ close to the exciton energy E_0, one gets

$$\varepsilon_{\pm}(\omega)=\varepsilon_1+\frac{2\pi e^2}{m^2\omega^2\Omega_0}\sum_{v,m}\sum_{c,m'}\frac{|\langle c,m'|p_{\pm}|v,m\rangle|^2}{\hbar\omega_{m'm}-\hbar\omega-i\Gamma} \tag{17}$$

(e is the electron charge; m is the electron mass; Ω_0 is the elementary cell volume). The summation in (17) runs over the conduction (c,m') and valence (v,m) states, split by the *sp-d* exchange interactions. $\hbar\omega_{m'm}$ is the energy difference $E_{c,m'}-E_{v,m}$ and ε_1 is the background dielectric constant involving contributions of other interband transitions; $p_{\pm}$ is the operator $p_x\pm ip_y$.

The allowed transitions contributing to ϵ_+ are

$$(3/2,-3/2)\rightarrow(1/2,-1/2)$$

and

$$(3/2,-1/2)\rightarrow(1/2,+1/2)\quad(\Delta m_J=+1),$$

while the contributions to ε_- arise from

$$(3/2,+3/2)\rightarrow(1/2,+1/2)$$

and

$$(3/2,+1/2)\rightarrow(1/2,-1/2)\quad(\Delta m_J=-1).$$

Therefore, the frequency-dependent dielectric function associated with each $\sigma^{\pm}$ mode is

$$\varepsilon_{\pm}=\varepsilon_1+\frac{4\pi e^2P^2}{m^2\omega^2\Omega_0}\left[\frac{1}{E_0\mp E_1/2-\hbar\omega-i\Gamma}+\frac{1/3}{E_0\mp E_2/2-\hbar\omega-i\Gamma}\right], \tag{18}$$

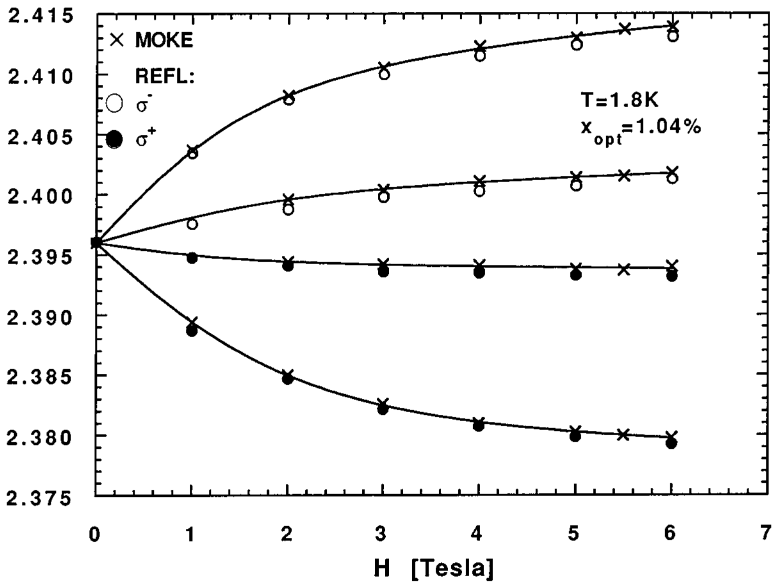

FIG. 11. Energies of four exciton components for $x=1.04\%$ sample at $T=1.8$ K. The crosses correspond to MOKE data, while open and filled circles to σ^- and σ^+ data, respectively. The solid line are guides for eyes.

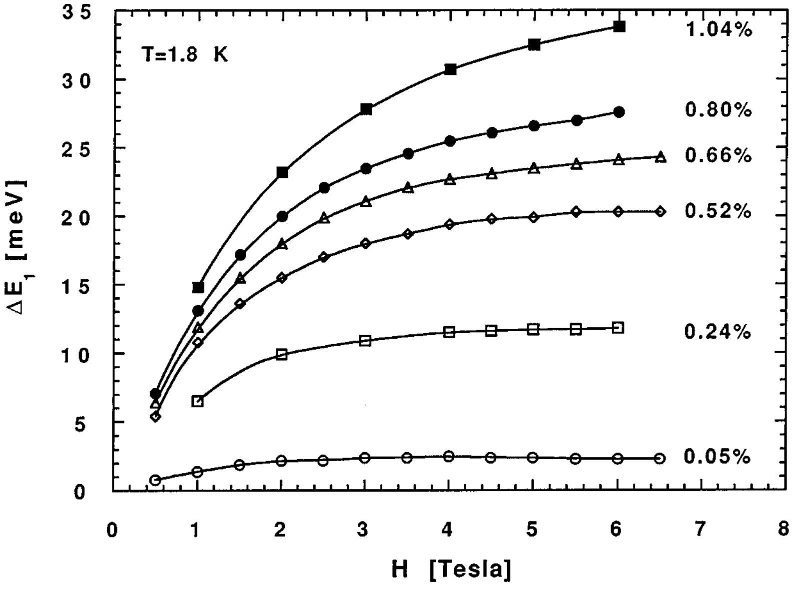

FIG. 12. Energy splitting of the strong exciton components vs field for different compositions ($T=1.8$ K). x_{opt} is reported on each curve. The solid lines are guides for eyes.

where E_1 and E_2 are the exchange energies

$$E_1=-N_0(\alpha-\beta)x\langle\langle S_z\rangle\rangle,$$

$$E_2=N_0(\alpha+\beta/3)x\langle\langle S_z\rangle\rangle, \tag{19}$$

$P=\langle S|p_x|X\rangle$ is the interband matrix element, and Γ is a damping term. $N_0\alpha$ and $N_0\beta$ are the exchange constants for the Γ_6 and Γ_8 bands, respectively.

The Kerr rotation

$$\theta_k(\hbar\omega)=\frac{1}{2}\arg\frac{r^-(\hbar\omega)}{r^+(\hbar\omega)} \tag{20}$$

should be calculated numerically from Eqs. (15), (16), (18), and (19) for a given set of parameters. An analytical expression of $\theta_k(\hbar\omega)$ may be obtained in the limit $|\varepsilon_\pm-\varepsilon_1|\ll\varepsilon_1$:

$$\theta_k(\hbar\omega)=\frac{2\pi e^2P^2}{m^2\omega^2\Omega_0\sqrt{\varepsilon_1}(1-\varepsilon_1)}\,\mathrm{Im}\left[\frac{1}{E_0-E_1/2-\hbar\omega-i\Gamma}-\frac{1}{E_0+E_1/2-\hbar\omega-i\Gamma}+\frac{1/3}{E_0-E_2/2-\hbar\omega-i\Gamma}-\frac{1/3}{E_0+E_2/2-\hbar\omega-i\Gamma}\right]. \tag{21}$$

The Kerr spectrum consists of four peaks associated with each of the allowed transitions. The peaks associated with transitions allowed for σ^+ and σ^- polarizations have opposite signs. The comparison between the reflectance (with $\sigma^\pm$ polarization) and Kerr rotation spectra is illustrated in Fig. 8 for Zn$_{0.9934}$Co$_{0.0066}$Te ($H=2$ T). The peaks of θ_k occur approximately at the center of the reflectance structures. θ_k is positive (or negative) for transition allowed in σ^- (σ^+) po-

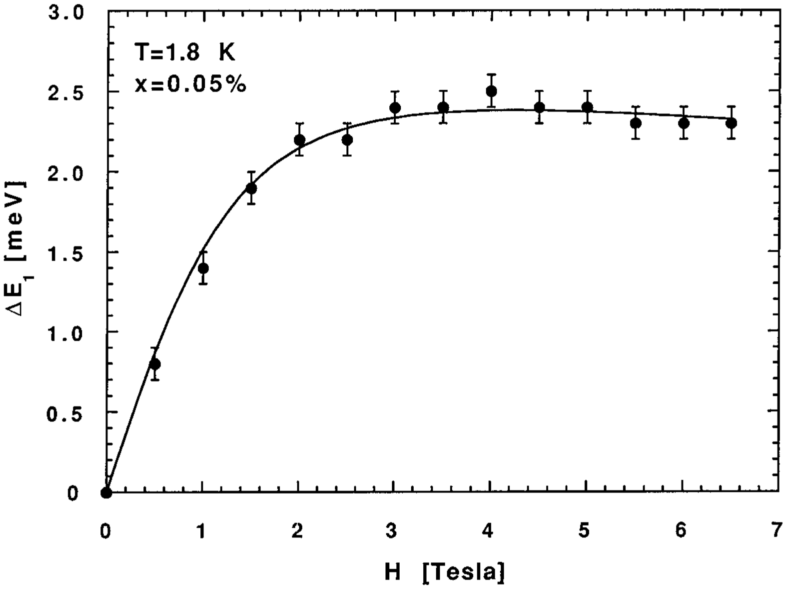

FIG. 13. Energy splitting of the strong exciton components vs field for $x=0.05\%$. Symbols are the experimental data. Solid line is the theoretical fit using Brillouin function+term linear in H [Eq. (24)]. The best fit corresponds to $g_e+6\kappa=-0.8$.

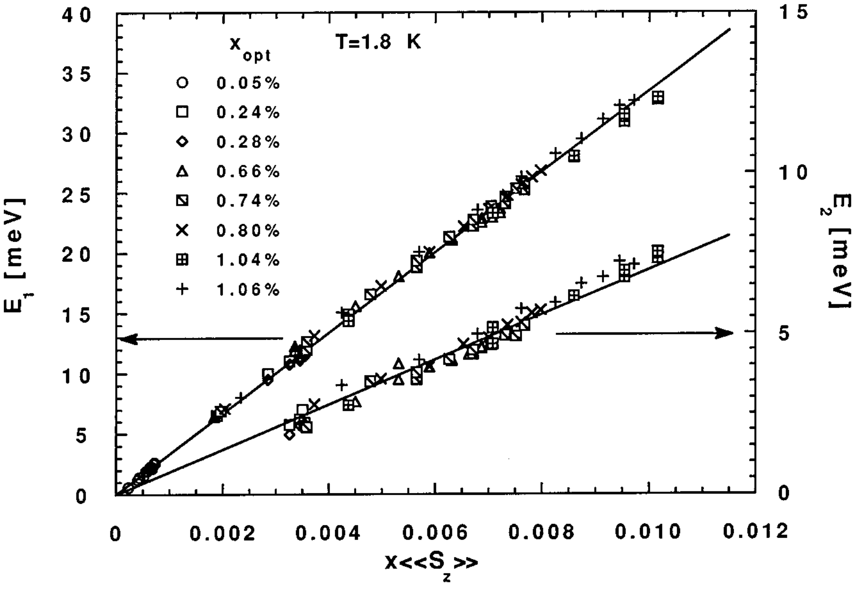

FIG. 14. Exchange energies E_1, E_2 vs $x\langle\langle S_z\rangle\rangle$ determined from magnetization measurements according to Eq. (2). The straight line represents the least-squares fit of Eqs. (19).

larizations. The Kerr rotation observed at resonance is quite large as compared to the results obtained in other magnetic systems.[16] The rotation reaches about 4° at the energy of the strongest transition ($-3/2\rightarrow-1/2$). This effect is the consequence of the strong circular magnetic birefringence induced by the Co-carrier exchange interactions.

Figure 9 shows the comparison between the Kerr rotation calculated from Eq. (20) with the experimental spectrum. Fits are made using damping terms and oscillator strengths as fitting parameters.

The Kerr rotation spectra obtained between 2.37 and 2.41 eV for different fields are displayed in Fig. 10. The amplitude of the peak associated with the lowest energy transition ($-3/2\rightarrow-1/2$) is nearly independent of the magnetic field whereas the peak corresponding to the ($3/2\rightarrow1/2$) transition is weakened and broadened with increasing field.

It is interesting to compare the theoretical expressions for the Kerr and Faraday rotations in the vicinity of the band edge. The Faraday rotation (per unit length)[22]

$$\theta_f = -\frac{\omega}{2\sqrt{\epsilon_1}c}\,\mathrm{Im}\,\varepsilon_{xy} \tag{22}$$

has the following form:

$$\theta_f = \frac{\pi e^2 P^2}{\sqrt{\epsilon_1}cm^2\omega\Omega_0}\,\mathrm{Re}\Bigg[\frac{1}{E_0-E_1/2-\hbar\omega-i\Gamma} - \frac{1}{E_0+E_1/2-\hbar\omega-i\Gamma} + \frac{1/3}{E_0-E_2/2-\hbar\omega-i\Gamma} - \frac{1/3}{E_0+E_2/2-\hbar\omega-i\Gamma}\Bigg]. \tag{23}$$

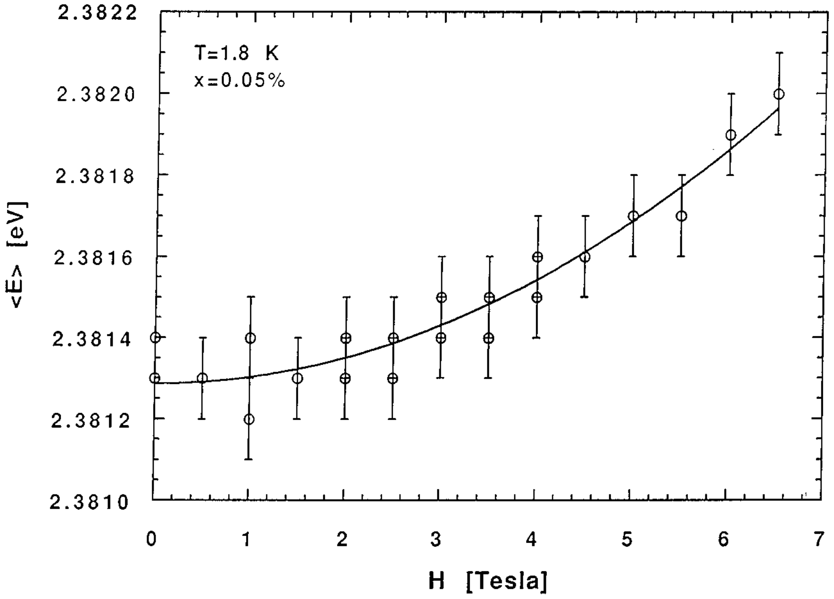

FIG. 15. The diamagnetic shift for the most dilute sample ($x=0.05\%$). Symbols are the average energy of $\sigma^{\pm}$ components. The solid line represents the best fit to the equation $\langle E\rangle = E_0+\sigma H^2$ with parameters $E_0=2.3813$ eV and $\sigma=1.6\times10^{-5}$ eV/T^2.

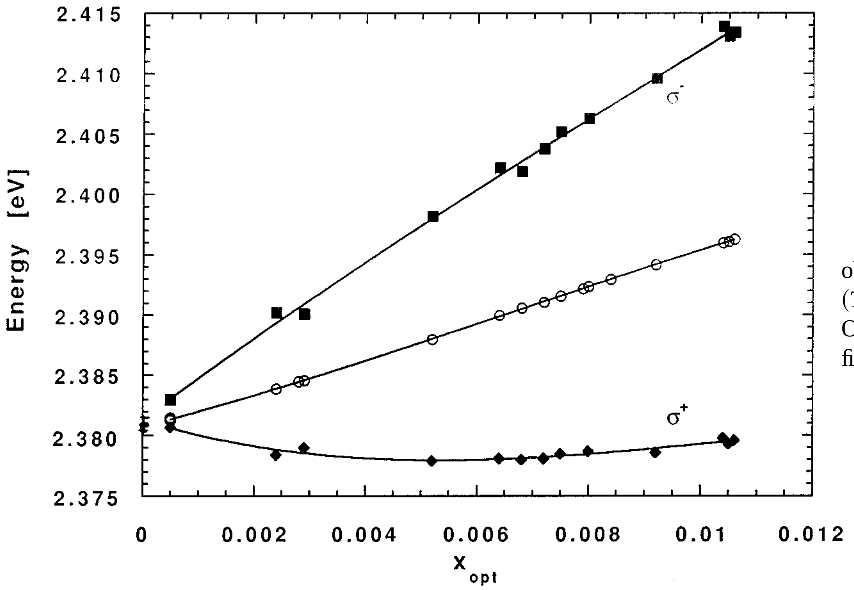

FIG. 16. Energies of the strong components observed in $\sigma^{\pm}$ polarizations in a field $H=6$ T ($T=1.8$ K) as a function of the Co composition. Open circles are the experimental data at zero field. Solid lines are guides for the eye.

Near a resonance transition, Faraday and Kerr effects exhibit either dispersion or absorption line shape. The peaks of the Kerr rotation are observed at the transition energy, while the extrema of θ_f are shifted with respect to the resonance position. The MOKE is particularly useful for determining precisely the transition energies, especially with low field, where the reflectance structures are weak. In contrast with the resonant Kerr effect, the observation of the resonant Faraday effect requires measurements on ultrathin samples, due to the large absorption coefficient at the band edge.

V. EXCHANGE SPLITTINGS

MOKE and magnetoreflectivity experiments have been performed, at $T=1.8$ K, to determine the sp-d exchange interactions. The four Zeeman components of the exciton state are observed for compounds of $x \geqslant 0.3\%$. Energies of the four transitions vs magnetic field are reported in Fig. 11 for $x=1.04\%$. For the most dilute compounds only the strong components were observed in $\sigma^{\pm}$ polarizations. The energy splitting ΔE_1 of the strong components vs magnetic field is shown in Fig. 12 for different Co compositions. We note in this figure the large splitting observed in $Zn_{1-x}Co_xTe$, as compared to that found in $Cd_{1-x}Co_xTe$ (Ref. 11) for the same Co composition. The ratio of the energy splittings $\Delta E_2/\Delta E_1$ is, within experimental accuracy, independent of magnetic field ($1.5 \leqslant H \leqslant 6.5$ T) and composition. We find $\Delta E_2/\Delta E_1 = 0.211 \pm 0.015$ in the entire composition range.

The experimental data are analyzed within the exchange model based on the mean-field approximation.[14] The splittings of the strong and weak components are, respectively,

$$\Delta E_1 = E_{(3/2\rightarrow 1/2)} - E_{(-3/2\rightarrow -1/2)}$$
$$= -N_0(\alpha-\beta)x\langle\langle S_z\rangle\rangle + (g_e^* + 6\kappa)\mu_B H, \tag{24}$$

$$\Delta E_2 = E_{(1/2\rightarrow -1/2)} - E_{(-1/2\rightarrow 1/2)}$$
$$= N_0(\alpha+\beta/3)x\langle\langle S_z\rangle\rangle + (2\kappa - g_e^*)\mu_B H. \tag{25}$$

The first term in (24) and (25) describes the exchange energies. The mean spin value $\langle\langle S_z\rangle\rangle$, as defined in Eq. (3), involves the contributions of three types of clusters (singles, pairs of second and third neighbors) included in the analysis of magnetization data. The last term in (24) and (25) represents the intrinsic Zeeman effect (g_e^* is the conduction band gyromagnetic factor and κ is the Luttinger parameter for Γ_8 valence bands). The intrinsic effect is apparent in Fig. 13, displaying the splitting ΔE_1 vs magnetic field for the most

TABLE II. sp-d exchange integrals (in eV), determined for several Co and Mn-based DMS.

	Cobalt					Manganese			
Lattice	x (%)	$N_0\alpha$	$N_0\beta$	$N_0(\alpha-\beta)$	Ref.	x (%)	$N_0\alpha$	$N_0\beta$	Ref.
CdTe	0.4			1.62	11	$x \leqslant 30$	0.22	−0.88	14
CdSe	1.1			2.52	9	5	0.26	−1.24	30
	2.0	0.27	−2.12	2.39	10	10	0.26		31
	4.8	0.28	−1.87	2.15	8	10;30	0.26	−1.11	32
	3.5	0.32			29				
ZnTe	0.05–1.06	0.31	−3.03	3.34	This work	$3.2 \leqslant x \leqslant 25$	0.18	−1.05	15
						$x \leqslant 9.5$	0.19	−1.09	33
ZnSe	1.0			2.42	12	$x \leqslant 10.3$	0.26	−1.31	34

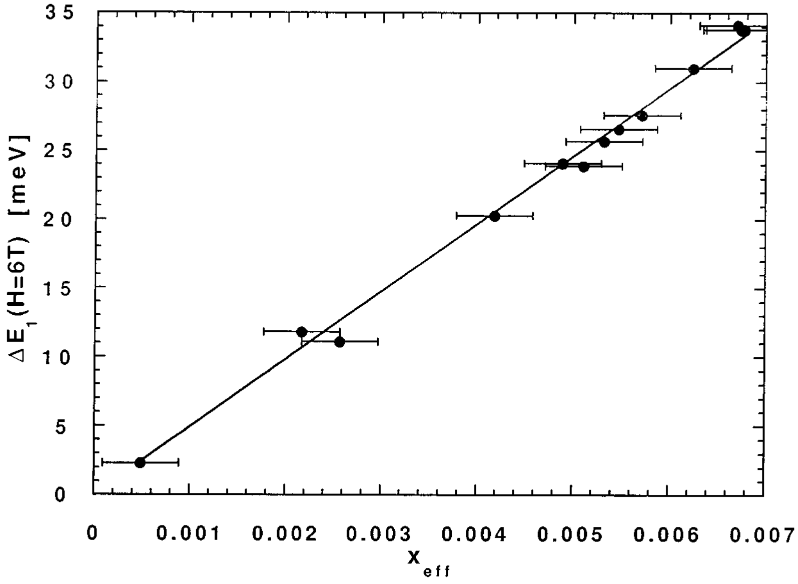

FIG. 17. Energy splitting ΔE_1 of the strong circular components, at $H=6$ T vs effective Co concentration $x_{\mathrm{eff}}=xP_1(x)$.

diluted compound. In the region, where the exchange contribution is saturated (above 4 T), ΔE_1 decreases with magnetic field. A least-squares fit of the data $\Delta E_1(H)$ to Eq. (24) provides an estimate of the intrinsic contribution: one gets $g_e^*+6\kappa=-0.8$. Using the value $g_e^*=-0.4$,[23] the contribution to ΔE_2 of the intrinsic Zeeman splitting is evaluated, $2\kappa-g_e^*=0.27$. Using these values we determine the exchange energies E_1 and E_2 [Eq. (19)] from ΔE_1 and ΔE_2 [Eqs. (24) and (25)] after subtraction of the intrinsic Zeeman splittings. These corrections are significant only for the most dilute compounds. For most samples, the term linear in H is negligible within experimental accuracy.

The exchange energies E_1 and E_2 are compared to the magnetization data obtained *on the same samples*, at $T=1.8$ K, for different values of the magnetic field. Figure 14 shows the dependence with $x\langle\langle S_z\rangle\rangle$ of both exchange energies. The proportionality of E_1 and E_2 to $x\langle\langle S_z\rangle\rangle$ is well verified over the entire field and composition range. From the least-squares fits of these data, we obtain

$$N_0(\alpha-\beta)=3.34\pm0.10 \text{ eV},$$

$$-N_0(\alpha+\beta/3)=0.70\pm0.06 \text{ eV}. \tag{26}$$

These data determine both exchange integrals

$$N_0\alpha=0.31\pm0.03 \text{ eV},$$

$$N_0\beta=-3.03\pm0.15 \text{ eV}. \tag{27}$$

The diamagnetic shift of the exciton is observed in the Zeeman spectrum of the most dilute compound ($x=0.05\%$). The average energy of the σ^+ and σ^- components, reported in Fig. 15, increases quadratically with the magnetic field. The diamagnetic shift is evaluated to be 1.6×10^{-2} meV/T^2. This result is comparable to the diamagnetic shift 2×10^{-2} meV/T^2 calculated from the model of Altarelli and Lipari,[24] for band parameters of ZnTe reported in Ref. 25.

Exchange parameters for Co-based DMS are reported in Table II with the corresponding values in Mn systems of identical lattice. The s-d exchange integral for ZnCoTe is comparable to that obtained for CdCoSe; $N_0\alpha$ is found to be larger in Co than in Mn-doped DMS. The p-d exchange interaction as well as the NN coupling constant J_1 are systematically stronger in Co than in Mn-based compounds of the identical host lattice. These differences may result from the lower S value of the Co^{2+} ion and from the location of the d levels relatively to the valence band.[26,27] The most spectacular result of the present study is the large p-d exchange constant found in ZnCoTe. The value $N_0\beta=-3.03$ eV deduced from the mean-field perturbation model exceeds considerably that found in CdCoSe.[8–10] The comparison between the values of $N_0(\alpha-\beta)$ for ZnCoSe,[12] CdCoTe,[11] and the present data corroborates the strong enhancement of sp-d exchange interactions in ZnCoTe. Moreover, the chemical trends found in Mn-based II-VI compounds are not verified in Co compounds (Table II): $N_0(\alpha-\beta)$ is found to increase as the host lattice changes from ZnSe to ZnTe (for the same Co concentration), in contrast with the trend observed in manganese selenides and tellurides.

In the case of Cd$_{1-x}$Co$_x$Se, the p-d exchange $|N_0\beta|$ increases with decreasing Co concentration (Table II). Similar behavior was observed in CdMnS:[28] the apparent p-d exchange interaction, deduced from exciton Zeeman splitting, exhibits an abnormally large magnitude for low Mn composition and an unusually strong dependence on x. This situation occurs when the exchange potential created by the localized magnetic ion is too weak to bind a hole but is too strong to be treated as a perturbation.[13] Calculations performed beyond the mean-field approximation (MFA) show that the multiscattering corrections to the valence energy level $m_J=3/2$, in saturating magnetic field, increase strongly at very low x, resulting in a composition dependence of the apparent value $|N_0\beta|$ and in asymmetrical splitting of the $\sigma^\pm$ components.[35]

In the present case, the large value of $|N_0\beta|$ obtained for ZnCoTe within the MFA might suggest that the multiscattering corrections should be taken into account in determination of the p-d exchange integral. Our results at saturation, however, do not provide evidence of asymmetric energy splittings of $\sigma^{\pm}$ transitions with respect to the zero-field transition, as shown in Fig. 16. In addition, the splitting at saturation ΔE_1 varies nearly linearly with the effective composition $x_{\mathrm{eff}}=xP_1(x)$ in diluted region (Fig. 17), indicating that the correction factors do not depend sensitively on concentration. If the multiscattering corrections exist, they are expected to be weaker than in CdMnS, as the hole effective mass is weaker.[13]

ACKNOWLEDGMENTS

We wish to thank C. Benoit à la Guillaume and A. Ghazali for fruitful discussions and for a careful reading of the manuscript. We are grateful to I. Rosenman for his efficient cooperation in SQUID experiments. We also acknowledge W. Szuszkiewicz who has performed x-ray fluorescence analysis on numerous samples and B. Witkowska for help in sample preparation. The Groupe de Physique des Solides is Unité de Recherche Associée au Centre National de la Recherche Scientifique.

---

[*] Permanent address: Institute of Physics, Polish Academy of Sciences, Al. Lotnikow 32/46, 02 668 Warsaw, Poland.

[1] A. Twardowski, H. J. M. Swagten, and W. J. M. de Jonge, in *II-VI Semiconductor Compounds*, edited by M. Jain (World Scientific, Singapore, 1993), p. 227.

[2] A. Lewicki, A. I. Schindler, J. K. Furdyna, and W. Giriat, Phys. Rev. B **40**, 2379 (1989).

[3] A. Lewicki, A. I. Schindler, I. Miotkowski, and J. K. Furdyna, Phys. Rev. B **41**, 4653 (1990).

[4] A. Lewicki, A. I. Schindler, P. M. Shand, B. C. Crooker, and J. K. Furdyna, Phys. Rev. B **44**, 6137 (1991).

[5] T. M. Giebultowicz, P. Klosowski, J. J. Rhyne, T. J. Udovic, J. K. Furdyna, and W. Giriat, Phys. Rev. B **41**, 504 (1990).

[6] T. M. Giebultowicz, J. J. Rhyne, J. K. Furdyna, and P. Klosowski, J. Appl. Phys. **67**, 5096 (1990).

[7] T. Q. Vu, V. Bindilatti, Y. Shapira, E. J. McNiff, Jr., C. C. Agosta, J. Papp, R. Kershaw, K. Dwight, and A. Wold, Phys. Rev. B **46**, 11 617 (1992).

[8] M. Nawrocki, F. Hamdani, J. P. Lascaray, Z. Golacki, and J. Deportes, Solid State Commun. **77**, 111 (1991).

[9] M. Inoue, N. Adachi, I. Mogi, G. Kido, and Y. Nakagawa, Physica B **184**, 441 (1993).

[10] U. Gennser, X. C. Liu, T. Q. Vu, D. Heiman, T. Fries, Y. Shapira, M. Demianiuk, and A. Twardowski, Phys. Rev. B **51**, 9606 (1995).

[11] O. W. Shih, R. L. Aggarwal, T. Q. Vu, and P. Becla, Solid State Commun. **81**, 245 (1992).

[12] X. Liu, A. Petrou, B. T. Jonker, J. J. Krebs, G. A. Prinz, and J. Warnock, J. Appl. Phys. **67**, 4796 (1990).

[13] C. Benoit à la Guillaume, D. Scalbert, and T. Dietl, Phys. Rev. B **46**, 9853 (1992); D. Scalbert, A. Ghazali, and C. Benoit à la Guillaume, *ibid*. **48**, 17 752 (1993).

[14] J. A. Gaj, R. Planel, and G. Fishman, Solid State Commun. **29**, 435 (1979).

[15] G. Barilero, C. Rigaux, M. Menant, Nguyen Hy Hau, and W. Giriat, Phys. Rev. B **32**, 5144 (1985).

[16] N. Sato, Jpn. J. Appl. Phys. **20**, 2403 (1981).

[17] M. Villeret, S. Rodriguez, and E. Kartheuser, Physica B **162**, 89 (1990).

[18] J. M. Baranowski, J. W. Allen, and G. P. Pearson, Phys. Rev. **160**, 627 (1967).

[19] F. S. Ham, G. W. Ludwig, G. D. Watkins, and H. H. Woodbury, Phys. Rev. Lett. **5**, 468 (1960).

[20] C. Testelin, C. Rigaux, A. Mauger, A. Mycielski, and M. Guillot, Phys. Rev. B **46**, 2193 (1992).

[21] G. Barilero, C. Rigaux, Nguyen Hy Hau, J. C. Picoche, and W. Giriat, Solid State Commun. **62**, 345 (1987).

[22] I. M. Boswarva, R. E. Howard, and A. B. Lidiard, Proc. R. Soc. London Ser. A **269**, 125 (1962).

[23] M. Drechsler, P. Emanuelsson, B. K. Meyer, H. Mayer, U. Rössler, and B. Clerjaud, Phys. Rev. B **50**, 2649 (1994).

[24] M. Altarelli and N. O. Lipari, Phys. Rev. B **7**, 3798 (1973).

[25] H. Mayer and U. Rössler, Solid State Commun. **87**, 81 (1993).

[26] B. E. Larson, K. C. Hass, H. Ehrenreich, and A. E. Carlsson, Solid State Commun. **56**, 347 (1985); Phys. Rev. B **37**, 4137 (1988).

[27] A. K. Bhattacharjee, Phys. Rev. B **46**, 5266 (1992).

[28] S. I. Gubarev and M. G. Tyazhlov, Pis'ma Zh. Eksp. Teor. Fiz. **44**, 385 (1986) [JETP Lett. **44**, 494 (1986)]. S. I. Gubarev and M. G. Tyazhlov, Fiz. Tverd. Tela (Leningrad) **32**, 635 (1990) [Sov. Phys. Solid State **32**, 373 (1990)].

[29] D. U. Bartholomew, E-K. Suh, A. K. Ramdas, S. Rodriguez, U. Debska, and J. K. Furdyna, Phys. Rev. B **39**, 5865 (1989).

[30] M. Arciszewska and M. Nawrocki, J. Phys. Chem. Solids **47**, 309 (1986).

[31] Y. Shapira, D. Heiman, and S. Foner, Solid State Commun. **44**, 1243 (1982).

[32] R. L. Aggarwal, S. N. Jasperson, J. Stankiewicz, Y. Shapira, and S. Foner, Phys. Rev. B **28**, 6907 (1983).

[33] A. Twardowski, P. Swiderski, M. von Ortenberg, and R. Pauthenet, Solid State Commun. **50**, 509 (1984).

[34] A. Twardowski, B. Dietl, and M. Demianiuk, Solid State Commun. **48**, 845 (1983).

[35] J. Tworzydlo, in *Proceedings of the European Workshop on II-VI Semiconductors and International Workshop on Semimagnetic (Diluted Magnetic) Semiconductors*, edited by H. Heinrich (Trans Tech, Switzerland, 1995) and Phys. Rev. B **50**, 14 591 (1994).